Coupling of electronic charge and spin at a ferromagnetic-paramagnetic metal interface

Mark Johnson and R. H. Silsbee
Laboratory of Atomic and Solid State Physics, Cornell University, Clark Hall, Ithaca, New York 14853-2501
(Received 22 June 1987)

Microscopic models are presented to elucidate the concept of interfacial charge-spin coupling. At the interface between a ferromagnet and a paramagnet, the spin subbands are loosely coupled, an interfacial conductance may be defined for each, and a result of their inequivalence is that an electric current flowing from a ferromagnetic metal into a paramagnetic metal will be partially spin polarized, i.e., will have an associated current of magnetization. The inverse is also true; nonequilibrium magnetization present in a paramagnetic metal can be detected as an open circuit voltage across an interface between the paramagnet and a ferromagnet. Using this effect, a new technique to measure conduction electron relaxation times is described.

I. INTRODUCTION

The purpose of this paper is to introduce a new concept. In the following paper we describe details of an experiment that demonstrates its viability while providing a new technique to measure the conduction electron-spin relaxation time T_2. The concept can be described in the following way. Historically, investigators have always related an electric current to a gradient (within bulk metal) of electric potential and, more generally, to a gradient in temperature. At an interface between two metals, the electric current is related to differences, across the interface, of the voltage and temperature. Similarly, they have always related a current of magnetization to a gradient (in the bulk) or difference (at an interface) of nonequilibrium magnetization. We propose, and our spin injection experiment[1] demonstrates, that in fact there exists a coupling between charge and spin, which implies the following at an interface between ferromagnetic and paramagnetic metals: a current of magnetization will exist in proportion to the voltage difference across the interface; and an electric current will be related to a difference in *magnetization potential*,[2] $-H^* \equiv (\tilde{M}/\chi) - H$, across the interface. In slightly different words, an electric current that is driven, by a difference in voltage, into the paramagnet from the ferromagnet will have associated with it a current of nonequilibrium magnetization that is driven into the paramagnet. By the same token, when nonequilibrium magnetization is induced in the paramagnet, the difference in magnetization potential at the interface with a ferromagnet results in an associated electric current (or a difference in voltage, if there is no external circuit connecting the ferromagnet to the paramagnet, or if they are connected by a high impedance voltmeter) across the interface. Although electronic-spin injection into metals has already been introduced,[3,4] the generalized idea of a coupling between charge and spin at an interface is a new concept; it has not been considered in previous treatments of magnetization transport.

Torrey[5] pioneered the study of the diffusion of nonequilibrium magnetization under the influence of an applied magnetic field gradient, using the particular system of a fluid of nuclear spins (of spin $\frac{1}{2}$). He showed that a current of nonequilibrium magnetization is given by

$$\mathbf{J}_M = -D\nabla(M - M_0) \equiv -D\nabla\delta M \ , \tag{1}$$

where D is the coefficient of self-diffusion, M is the magnetization (magnetic moment per unit volume), $M_0 = \chi H$ is the equilibrium magnetization (which is proportional to the applied field H), χ is the volume susceptibility, and δM is the nonequilibrium magnetization. These ideas pertained to the flow of nonequilibrium magnetization in a continuous material.

Flesner, Fredkin, and Schultz,[6] and Magno and Pifer[7] have studied bimetal systems by electron-spin resonance (ESR) and transmission electron-spin resonance (TESR), with the goal of analyzing interfacial electronic charge and spin transmission. The former authors proposed general boundary conditions for transverse magnetization at the interface between two paramagnetic (at least *not* ferromagnetic) metals, metal $i = 1,2$. Within the bulk, on either side of the interface, there is, from Eq. (1), a current of magnetization $(\mathbf{J}_M)_i = -D\nabla\delta M_i$. A difference of $\delta M/\chi$ (where χ is the static susceptibility) across the interface

$$\left[\frac{\delta M}{\chi}\right]_1 - \left[\frac{\delta M}{\chi}\right]_2 \neq 0$$

will contribute to a current of magnetization across the interface. There may also be relaxation processes at the interface which destroy magnetization (a *sink* of magnetization) so that the net magnetization current in the bulk may be different on each side of the interface. Flesner *et al.* choose phenomenological coefficients b_{ij} to relate $(\mathbf{J}_M)_i$ to $(\delta M/\chi)_i$, and demand conservation of magnetic current (including the effect of sinks at the interface) to arrive at boundary equations for the interface:

$$\frac{-D_1\nabla\delta M_1}{\gamma_1} = b_{11}\frac{\gamma_1\delta M_1}{\chi_1} + b_{12}\frac{\gamma_2\delta M_2}{\chi_2} \ , \tag{2}$$

and

$$\frac{D_2\nabla\delta M_2}{\gamma_2}=b_{21}\frac{\gamma_1\delta M_1}{\chi_1}+b_{22}\frac{\gamma_2\delta M_2}{\chi_2}\ ,$$

where for metal i, δM_i is the nonequilibrium magnetization $\delta M_i=g_i\beta\Delta n_i/2$, γ is the gyromagnetic ratio $\gamma=g\beta/\hbar$, β is the Bohr magneton, g is the g factor (spectroscopic splitting factor), and Δn_i is the number density of nonequilibrium spins. In describing the general case where nonequilibrium magnetization is an oscillating function of time, the b_{ij} could be complex. In their analysis, Flesner *et al.* take the b_{ij} to be real, and require $b_{12}=b_{21}$ by detailed balance.

The coefficients b_{ij} are not simply related to transmission or reflection probabilities. One may gain a little bit of insight into their meaning by the examination of limiting cases. When $b_{12}=0$ there is no spin-spin coupling across the interface, and the interface acts like a sink of magnetization. The surface relaxation rates are described by b_{11} and b_{22} for the respective sides of the interface. The relaxation rate is measured (from the increased linewidth, the procedure is briefly described in a coming section) by reflection electron-spin resonance from *both* sides of the bimetal sample. If $|b_{12}|$ is large (b_{12} may include both direct and indirect spin transfer; in the former case, a spin is physically transported from one side to the other, in the latter case a torque is applied between spins across the interface), magnetization may be transmitted across the interface. This is called the strong coupling limit, and one can only deduce an overall interface relaxation parameter $R=b_{11}+b_{22}+2b_{12}$. This is measured (from the line shape and a computer fit) by transmission electron-spin resonance through the bimetal sample; a broadened TESR line is observed at the average g value of the two metals.[8]

Prior to the work presented in this article (excepting Aronov's proposal), the transport of charge and the transport of magnetization across a bimetal interface have always been treated independently; an electric current is driven by a difference in voltage, and a current of magnetization is driven by a difference in nonequilibrium magnetization at the interface. The concepts presented herein assert, and the spin injection experiment described in the following paper demonstrates, that these transport processes are not independent. Rather, a difference in voltage at a ferromagnetic-paramagnetic interface will drive a magnetization current, and a difference in magnetization potential will drive an electric current. Charge and spin are coupled at the interface, cross terms must be included in describing the transport processes, and thus Eqs. (2) need to be generalized to include a term proportional to the electric potential difference across the interface. Similarly, the electric current density must contain a term proportional to the difference across the interface of the magnetization potential. The bulk transport equations [Eq. (1) and Ohm's Law] need to be generalized, as well, to include terms proportional to an electric field and $\delta M/\chi$. In a bulk ferromagnet this term may be large. In a bulk paramagnet it is negligible. At the interface of a paramagnet with a ferromagnet, it is equally important as the other terms in Eqs. (2).

Aronov was the first to suggest, in Ref. 3, that spins could be driven into a bulk metal at a ferromagnetic-paramagnetic interface. Tedrow and Meservey had earlier demonstrated that spins can be injected into the quasiparticle states of a superconducting film.[4,9,10] Silsbee[11] extended the idea of charge-spin coupling, and proposed that a nonequilibrium magnetization in a paramagnet will result in an associated voltage step across the interface with a ferromagnet. This proposal motivated the spin injection experiment. In another article,[2] the authors have used the formalism of nonequilibrium thermodynamics to identify the magnetization potential as the thermodynamic variable associated with the flow of nonequilibrium magnetization, and developed the linear dynamic equations of motion for a system of particles that carry charge, kinetic energy, and magnetic moment under the influence of differences (or gradients) of voltage, temperature, and magnetization potential. The relevance of charge-spin coupling to bulk transport processes is developed in that publication. In this paper microscopic models will be used to elucidate the idea of a coupling between electronic charge and spin at ferromagnetic-paramagnetic interface ("interfaces" are taken to be of limited conductance; further remarks are found in the subsequent article). We will see that one can "tag" electrons with a magnetic moment and detect the tagged particles at other positions in the material. Using this concept we have created a new nonresonance technique, which is described in Sec. III, to measure conduction electron T_2's in zero field. In Appendix A some of the ideas used in discussing interfacial transport are formally developed. Appendix B contains a solution to the Bloch equations with a diffusion term. In the following article we offer details of the spin injection experiment: we describe the cryostat and samples, present and analyze typical data, and discuss the results within the framework of concepts developed herein.

II. THE CONCEPT

In this section we will first investigate how spins can be injected from a ferromagnet into a paramagnet. Next we examine how the injected nonequilibrium spins behave within the paramagnet. Finally, we will see what happens when the nonequilibrium spins in the paramagnet are in interfacial contact with a second ferromagnet. The geometry of a pedagogical model is depicted in Fig. 1. In the middle is a slab of bulk paramagnetic metal of thickness L. On either side, a thin ferromagnetic film, each a single domain whose axis of magnetization is confined to lie in the plane but may be chosen in any direction in that plane, is in interfacial contact with the paramagnet. We choose the axis of magnetization of the left film to point up. When a switch is closed, a battery drives a current through the film into the bar. On the right, we may choose an impedance Z to connect the second film to the bottom of the slab via an external circuit.

A. Injection

Consider the interface between the left ferromagnetic film and the paramagnetic metal. Figure 2(a) represents

an overidealized Stoner ferromagnet, on the left, in equilibrium with a free electron paramagnet on the right before the switch is closed. Now apply an electric potential V_0 across the interface to drive a current from left to right [refer to Fig. 3(a)]. Aronov proposed that if the Fermi surface in the ferromagnet lies entirely within one spin subband, then the current would be carried entirely by electrons of that spin orientation. Magnetization would be injected into the paramagnet at a rate proportional to the electric current. Associated with the transfer across the interface of each electric charge e is the transport of a magnetization β, where β is the Bohr magneton. The injected magnetization current[12] J_M associated with the electric current J_e is trivially argued to be the number current of carriers, J_e/e, multiplied by the magnetic moment β that each carries:

$$J_M = \frac{\beta}{e} J_e \ . \tag{3}$$

For a real ferromagnet the Fermi surface will contain both spin subbands, but in a substantial imbalance [Fig. 2(b)]. The reduced efficiency of magnetization injection is described by a dimensionless phenomenological coefficient $\eta < 1$,

$$J_M = \frac{\eta\beta}{e} J_e \ . \tag{4}$$

If the spin subbands are weakly coupled to each other, and spin relaxation at the interface is neglected, an interfacial conductance per unit are, $g_{\rm up}^{\rm down}$, may be defined (an expression is developed in Appendix A) for each. The parameter η may then be defined in terms of sums and differences of $g_{\rm down}$ and $g_{\rm up}$. This follows directly from a calculation of the magnetization injected from a nonideal ferromagnet into a paramagnet for the simple case of a Stoner ferromagnet with subband imbalance and for a paramagnet whose band structure is free-electron like. It will help to refer to Fig. 3(e). In this figure a voltage is applied across the interface of a nonideal ferromagnetic film and a paramagnetic metal, and the paramagnet with nonequilibrium magnetization is in interfacial contact with a second nonideal ferromagnet [Fig. 3(f)]. Current can flow between the "up" subbands of the paramagnet and ferromagnet, and between the "down" subbands of the two materials. In Fig. 3(e) current flows from the up-spin subband of the ferromagnet to the up-spin subband of the paramagnet (the dotted line above $E_{F;p,\rm up}$) and charge neutrality requires an equivalent loss from the down-spin subband (the dotted line below $E_{F;p,\rm down}$).

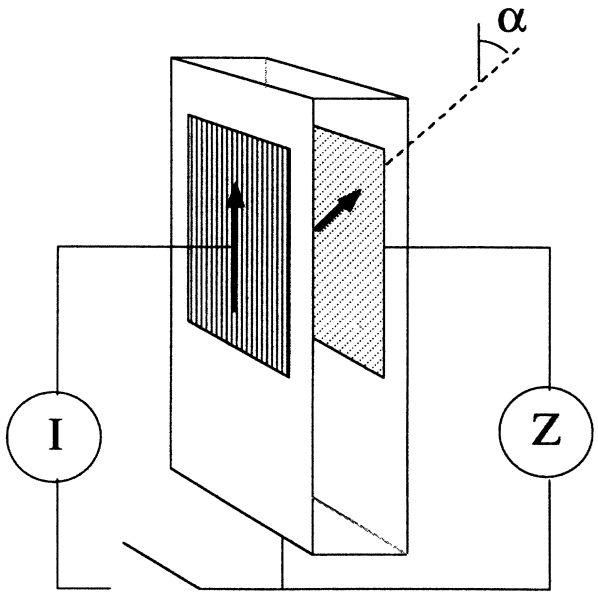

FIG. 1. An illustration to demonstrate charge-spin coupling at the interface between a ferromagnet and a paramagnet. A ferromagnetic film is on each side of a thin slab of bulk paramagnetic metal. The films are taken to be single domains and the magnetization lies in the plane of the films. In most of the discussion the films are aligned ($\alpha = 0°$). A current is driven through the left ferromagnetic film into a bulk paramagnet of thickness L less than δ_s. Some fraction of the injected electrons are spin polarized. In the paramagnet, the electrons diffuse randomly and lose spin memory in a time T_2. A nonequilibrium magnetization δM results in the paramagnet. If Z is a low impedance ammeter, a current will flow through Z that is proportional to δM. If Z is a high impedance voltmeter, it will measure a voltage that is proportional to δM.

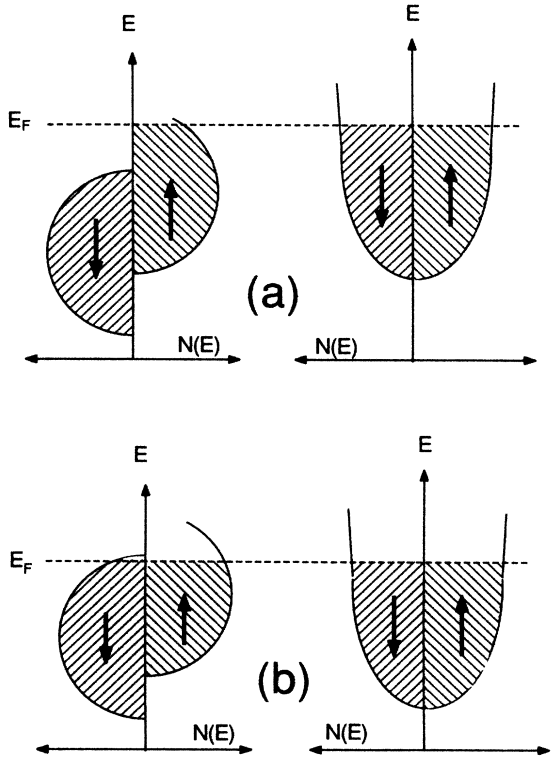

FIG. 2. (a) The density of states of the 3d band of an idealized Stoner model transition-metal ferromagnet (on the left) in equilibrium with the free-electron density of states of a (Pauli) paramagnetic metal. (b) The Fermi surface of a nonideal Stoner ferromagnet will contain both spin subbands, but in a substantial imbalance.

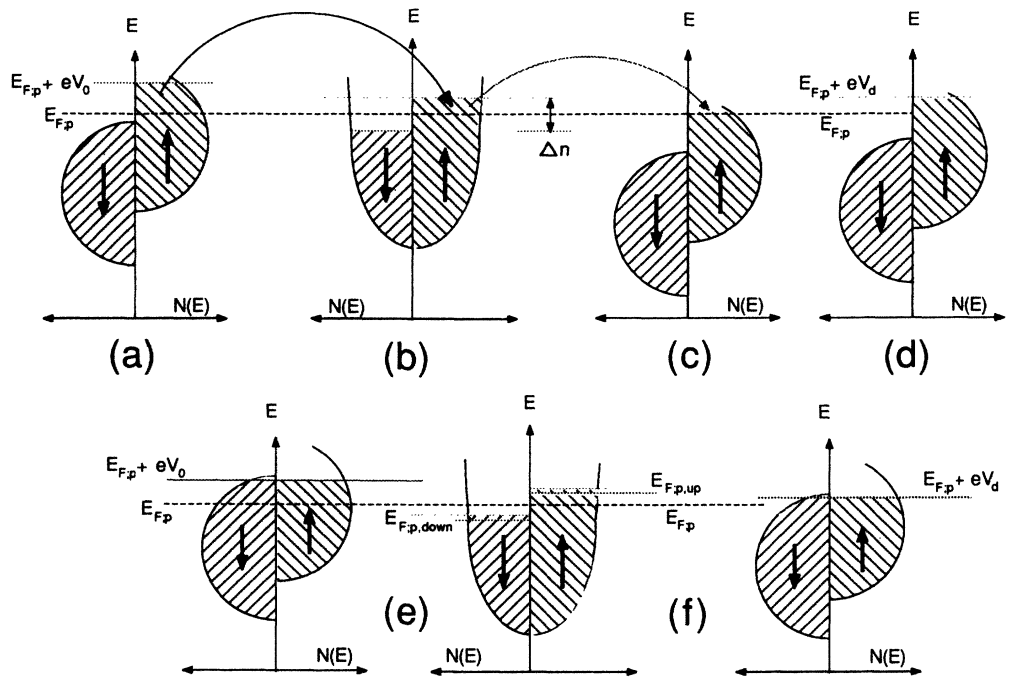

FIG. 3. An ideal Stoner ferromagnet is in interfacial contact with a paramagnet of thickness less than δ_s. The back surface of the latter is in interfacial contact with a second ideal ferromagnet (see also the pedagogical model of Fig. 1). (a) A voltage $-V_0$ is applied across the interface to drive a current into the paramagnet. (b) Associated with the current is a current of magnetization, and a nonequilibrium magnetization results in the paramagnet, $\delta M=\beta\Delta n$. (c) If the film and paramagnet are externally connected by a low impedance wire, an electric current will flow across the second interface in proportion to δM. (d) If they are externally connected through a high impedance circuit, then the Fermi surface of the second ferromagnet will align with the nonequilibrium spins in the paramagnet. (e) An injector junction with a nonideal ferromagnet. The subbands are in substantial imbalance, and are weakly coupled so that an interfacial conductance for each subband may be defined. Current flows from the down- (up-) spin subband of the ferromagnet to the down- (up-) spin subband of the paramagnet, and charge neutrality requires an equivalent loss from the up- (down-) spin subband. (f) A detector junction with a nonideal ferromagnet. If an external circuit connects the two metals with a low impedance ammeter, currents will flow across the interface between down-spin subbands (right to left) and up-spin subbands (left to right). If a large impedance voltmeter is placed in the external circuit, the Fermi level of the ferromagnet will be raised an amount eV_d, calculated in the text.

There is also current flow from the down-spin subband of the ferromagnet to the down-spin subband of the paramagnet resulting in the down-spin subband chemical potential $E_{F;p,\text{down}}$. Again, charge neutrality requires an equivalent loss from the up-spin subband, and the up-spin subband chemical potential $E_{F;p,\text{up}}$ is the result.

In Appendix A we derive the following expression for the interfacial conductance per unit area g_s for current from the subband s (where s is up or down) of the ferromagnet into the paramagnet [Eq. (A9)]:

$$g_s=\frac{e^2}{2}[N(E_F)\langle v_x\rangle\langle t\rangle]_{i,s} , \tag{5}$$

where $N_s(E_F)$ is the density of states at the Fermi surface, $\langle v_x\rangle$ is an (angular) average of the component of Fermi velocity perpendicular to the interface [defined in Eq. (A7)], $\langle t\rangle$ is a probability that an electron is transmitted from the ferromagnet, across the interface, and into the paramagnet [defined in Eq. (A8)], and these three quantities are evaluated in the ferromagnet (i.e., $i=f$). One could follow an analogous argument to solve for the conductance for current from the paramagnet into the ferromagnet. The result would be Eq. (5), where now the quantities in the square brackets are evaluated in the paramagnet. In other words, detailed balance requires

$$[N(E_F)\langle v_x\rangle\langle t\rangle]_{p,s}=[N(E_F)\langle v_x\rangle\langle t\rangle]_{f,s} . \tag{6}$$

If the ferromagnet were ideal [Fig. 3(a)], then $g_{\text{down}}=0$. For a nonideal ferromagnet, $g_{\text{up}}\neq g_{\text{down}}$.

Assuming that relaxation within the spin subbands (characterized roughly by an inelastic resistivity scattering time) is rapid compared with relaxation between subbands (the spin relaxation time), separate "quasi Fermi levels" may be usefully defined for each of the spin subbands. Let $E_{F;i,s}$ be the Fermi energy of the subband s (up or down) of the material i (f or p). For the injector [Fig. 3(e)], suppose a voltage $-V_0$ is applied across the interface. Assuming rapid spin relaxation within the ferromagnet, the magnetization in the ferromagnet remains in equilibrium,

$$E_{F;f,\mathrm{up}}=E_{F;f,\mathrm{down}}=E_{F;p}+eV_0 \ , \tag{7}$$

where $E_{F;p}$ is the average Fermi level of the two subbands in the paramagnet, and for a negative voltage the chemical potential in the ferromagnet is raised by $(-e)(-V_0)$ relative to that in the paramagnet. Then the electric current from the ferromagnet to the paramagnet is

$$J_e=\frac{1}{e}[g_{\mathrm{up}}(E_{F;f,\mathrm{up}}-E_{f,p})+g_{\mathrm{down}}(E_{F;f,\mathrm{down}}-E_{F;p})]$$

$$=(g_{\mathrm{up}}+g_{\mathrm{down}})V \ . \tag{8}$$

The magnetic current from the ferromagnet to the paramagnet is

$$J_M=\frac{\beta}{e}[g_{\mathrm{up}}(E_{F;f,\mathrm{up}}-E_{F;p})-g_{\mathrm{down}}(E_{F;f,\mathrm{down}}-E_{F;p})]$$

$$=\frac{\beta}{e}(g_{\mathrm{up}}-g_{\mathrm{down}})V \ . \tag{9}$$

The ratio of J_M to J_e is

$$\frac{J_M}{J_e}=\frac{g_{\mathrm{up}}-g_{\mathrm{down}}}{g_{\mathrm{up}}+g_{\mathrm{down}}}\frac{\beta}{e}\equiv\eta\frac{\beta}{e} \ , \tag{10}$$

which defines η,[13] under the assumption of no interfacial spin relaxation, by comparison with Eq. (4). Notice that if either g_{up} or $g_{\mathrm{down}}\rightarrow 0$ (which implies an ideal ferromagnet), then $|\eta|\rightarrow 1$, and we have the result of Eq. (3).

We can generalize this somewhat, and allow the ferromagnet to have more than one band b at the Fermi surface. Then let the parameter η_b describe the transport of spin polarized current from band b of the ferromagnet across the interface and into the paramagnet. We define η_b as the ratio, for band b, of the difference between two interfacial current contributions (that with carriers whose magnetic moments are aligned with the direction $\hat{m}$ of equilibrium magnetization in the ferromagnetic film, and that whose carriers are antialigned with $\hat{m}$) to the total interfacial current contribution of band b:

$$\eta_b=\frac{J_{b,\mathrm{up}}-J_{b,\mathrm{down}}}{J_{e,b}}=\frac{g_{b,\mathrm{up}}-g_{b,\mathrm{down}}}{g_{b,\mathrm{up}}+g_{b,\mathrm{down}}} \ . \tag{11}$$

The total interfacial current is

$$J_e=\sum_b J_{e,b} \ ,$$

and the parameter η for the total interfacial magnetization transport associated with electric current J_e is

$$\eta=\sum_b \eta_b\frac{J_{e,b}}{J_e} \ . \tag{12}$$

Note that if several bands contribute to the interfacial current transport, one band may be highly polarized ($\eta_{3d}\approx 1$, for example), but the net magnetization transport may be small ($\eta\ll 1$) if $J_{e,3d}/J_e\ll 1$ and the other band(s) is (are) weakly polarized.

Tedrow and Meservey[9,10] have demonstrated spin injection by using a dc tunneling conductance method. The quasiparticle density of states of thin films of metals with small spin-orbit interaction is Zeeman split by magnetic fields. In high fields this splitting can be resolved by a tunneling conductance measurement. If the other electrode is a ferromagnet, the imbalance of spin subbands will cause a preferential tunneling into the spin up (or spin down) quasiparticle states. One can deconvolve the asymmetry of the tunneling conductance characteristic to deduce the spin polarized current parameter "η." Meservey *et al.*[4] measured values of η from 0.1 to 0.5 for iron-nickel alloys for the tunneling process. Their results indicated that the injected magnetization was from the majority band, i.e., parallel to the ferromagnetic magnetization. In comparing different experiments, each purporting to measure η, one must recognize that there may be different mechanisms dominating the interfacial conductance. Remarks concerning a comparison of our results with those of Meservey *et al.* will be found in the following article.

B. Transport

Let us now turn our attention to a description of the behavior of the nonequilibrium spins that have been injected into the paramagnet. Figure 3 represents a steady-state process wherein a magnetic current is driven from a ferromagnet into a paramagnet. In Fig. 3(a) a potential $-V_0$ is applied across the interface, only the electrons of one spin subband are available to carry the current, and (as described above) there is an associated current of magnetization into the paramagnet. In the steady state, charge neutrality demands that some down spins are lost to compensate for the injected up spins. The magnetization diffuses away from the interface, and eventually relaxes by T_2 processes (in the limit of zero external field there is no distinction between transverse and longitudinal relaxation events, i.e., $T_2=T_1$). A useful parameter is the spin diffusion depth, $\delta_s=\sqrt{2DT_2}$, where D is the electronic diffusion constant. The spin depth δ_s is the average distance an electron travels before its spin is randomized by a collision. Within a spin depth of the interface, some steady-state nonequilibrium magnetization δM results [Fig. 3(b)] as a balance between the rate of magnetization injection (a *source* of magnetization) and the rate of destruction of magnetization by T_2 processes (a *sink* of magnetization). The nonequilibrium magnetization occupies a volume Ω defined by some combination of the sample parameters and δ_s, and the equality of injection and relaxation rates in the steady state implies

$$\delta M\approx I_m\frac{T_2}{\Omega}=\beta\Delta n \ , \tag{13}$$

where Δn is the difference in number density between up and down spins.

C. Detection

How might one detect this nonequilibrium magnetization? The answer is simple[11] and provides some new insight on the nature of interfaces. There is an inverse ar-

gument to that for the injector. If a second paramagnet is in interfacial contact with the paramagnet that has some nonequilibrium magnetization, its chemical potential will align with the average [$E_{F;p}$ in Fig. 3(b)] of the two spin subbands, and, because of the stringency of the charge neutrality condition, will be uninfluenced by the δM. However, consider the case of an ideal ferromagnet placed, on the right, in interfacial contact with the paramagnet. Again, due to the weak coupling (in the absence of interfacial relaxation) between spin subbands, an interfacial conductance exists for each subband. This is just the inverse of the injector picture. If an external circuit were to allow a current to pass from paramagnet to ferromagnet, i.e., Z a low impedance ammeter, only carriers in one spin subband will be available for the transport process. This is depicted in Fig. 3(c); there is a current through the interface which is proportional to the nonequilibrium magnetization in the paramagnet. More formally, we can say that a difference, across the interface, in the ratio of nonequilibrium magnetization to the susceptibility $(\delta\mathbf{M}/\chi)_p-(\delta\mathbf{M}/\chi)_F$ (equivalently one can think of a difference in the number of nonequilibrium spins) will drive a particle current. We suppose the ferromagnetic material to have a short enough relaxation time that the magnetization in the ferromagnetic film is always in equilibrium, or $(\delta M/\chi)_F\approx 0$. We see that an ammeter inserted at Z would measure an electric current proportional to the nonequilibrium magnetization δM_p. Note that if δM_p were of the opposite sign (if the down-spin subband were high and the up-spin subband low), the current would be of the same magnitude but would flow in the opposite direction. If this external circuit is now opened, i.e., if one chooses a high impedance for Z, the effect will be to raise the Fermi surface at the second film by an amount eV_d that is sufficient to prevent the difference in $\delta M/\chi$ at the interface from driving a current past this second film. This is depicted in Fig. 3(d). Hence, a high impedance voltmeter would measure an electric voltage V_d proportional to the magnetization in the paramagnet, and such an idealized ferromagnetic film can be used as a magnetization detector, as well as a magnetization injector.

One can think of a ferromagnetic film as a spin polarizer, and make an analogy to polarized light experiments. Suppose an electric current, initially of equal numbers of spin up and spin down electrons, is driven through the ideal ferromagnetic film on the left in Fig. 1. The film preferentially passes electrons of a particular spin orientation into the paramagnetic material. Note that we must not draw the analogy to a light polarizer too closely. The ferromagnetic film is many mean-free-paths thick and we do not mean to imply that any particular electron will be instantaneously transmitted or reflected, nor to imply that a "beam" of electrons is transmitted ballistically through the sample. However, the notion of a current that enters the film on one side with random spin orientation but leaves the other side with a net polarization along the axis of magnetization of the film may be conceptually useful. The second film, on the right in Fig. 1, works in the same way as a spin analyzer. Spins from a nonequilibrium magnetization in the paramagnet that are incident on the second film will pass through the analyzer, if they are aligned with its magnetization, and be detected as a current by a low impedance ammeter, or as a raised chemical potential by a high impedance voltmeter. Now imagine that the direction (axis) of magnetization of each film can be independently manipulated (in reality, this is true to an extent). The two films are in parallel planes, and the magnetization is confined to lie in the plane. Beginning with the two axes aligned, there is a maximum of current through the second film. As either of the axes is rotated, a current of equal magnitude but opposite sign through the second film will occur when the axes are antialigned ($\alpha=\pi$). In between aligned and antialigned, the current through the second film will be proportional to the projection $\cos\alpha$ of one axis on the other. Indeed, measuring detector current (or voltage) as a function of angle α would be one way of demonstrating the spin-charge coupling, and data from this kind of measurement are presented in the following paper.

We can calculate the detector voltage V_d in a straightforward way. Please refer to Figs. 3(b) and 3(d), and note that for an ideal Stoner ferromagnet, the Fermi surface of the detecting film will align with the top of the spin up subband of the paramagnet. Therefore, V_d can be calculated in the paramagnet, where one can make use of simple free-electron expressions. The energy eV_d will be the difference between the top of this band and $E_{F;p}$, a difference which is proportional to the number of nonequilibrium spins $\Delta n=\delta M/\beta$. The relationship between Δn and V_d is given by[14]

$$\frac{\delta M}{\beta}=\Delta n=2\int_{E_{F;p}}^{E_{F;p}+eV_d} N_{\rm up}(E)dE \ . \tag{14}$$

Assume that V_d is small, and that $N_{\rm up}(E)$, the density of states of a single spin subband of the paramagnet, is approximately constant and equal to $N_{\rm up}(E_F)$. We find

$$\frac{\delta M}{\beta}=N(E_F)eV_d=\frac{\chi}{\beta^2}eV_d \ , \tag{15}$$

where $N(E_F)$ is the density of states at E_F for both subbands, which gives

$$V_d=\frac{\beta\,\delta M}{e\chi} \ . \tag{16}$$

Here χ is the Pauli paramagnetic susceptibility,

$$\chi=\frac{\beta^2 m k_F}{\hbar^2\pi^2}=\beta^2 N(E_F) \ , \tag{17}$$

for free electrons.

For a nonideal ferromagnetic detector, it is easier to conceptualize the process and perform the calculation by thinking of the *current* from the paramagnet to the ferromagnet. Recall our comments and results of Sec. II A and Appendix A. In Fig. 3(f), $E_{F;p}$ is still the average Fermi level of the spin subbands of the paramagnet. Nonequilibrium magnetization has caused a different occupation for the subbands, and the chemical potential of the subbands is given by

$$\left.\begin{matrix} E_{F;p,\mathrm{up}} \\ E_{F;p,\mathrm{down}} \end{matrix}\right\} = E_{F;p} \pm \frac{\beta \delta M}{\chi} \ . \tag{18}$$

Suppose that an external circuit exists and a current flows. The current from the paramagnet to the ferromagnet is given by

$$J_e = \frac{1}{e}[g_{\mathrm{up}}(E_{F;p,\mathrm{up}} - E_{F;f}) + g_{\mathrm{down}}(E_{F;p,\mathrm{down}} - E_{F;f})] \tag{19}$$

$$= \frac{1}{e}\left[(E_{F;p} - E_{F;f})(g_{\mathrm{up}} + g_{\mathrm{down}}) + \frac{\beta \delta M}{\chi}(g_{\mathrm{up}} - g_{\mathrm{down}})\right] . \tag{20}$$

In Eq. (19) we see that there is a forward (paramagnet to ferromagnet) current between the spin up subbands, and a back (ferromagnet to paramagnet) current between the spin down subbands. When a high impedance voltmeter is inserted in the external circuit, no current flows ($J_e = 0$), and we get

$$-\frac{1}{e}(E_{F;p} - E_{F;f}) = \frac{\beta \delta M}{e\chi} \frac{g_{\mathrm{up}} - g_{\mathrm{down}}}{g_{\mathrm{up}} + g_{\mathrm{down}}} \ .$$

From Fig. 3(e) we identify the left-hand side as V_d, and from Eq. (10) we identify the right-hand side to achieve

$$V_d = \frac{\eta \beta \delta M}{e\chi} \ . \tag{21}$$

Here the g_s are defined in terms of the paramagnet, but, by detailed balance [Eq. (7)] they must be the same as in the ferromagnet. We thus learn that, under the assumption of no spin relaxation at the interface, the magnetization transport parameter η is the same for injection as for detection.

In another paper,[2] the equality of injection and detection efficiencies is derived more generally using an Onsager relationship in a linear-response formalism. Also note that the spin injection experiment is not sensitive to the sign of η because δM, in Eq. (21), is also proportional to η so that V_d is proportional to η^2. The sign of η could be measured in a different experiment. For example, δM could be created by a static field and saturation by microwaves tuned to the conduction electron-spin resonance. Then the voltage at a detector film would be linear in η.

III. MEASUREMENT OF T_2

Historically, electronic-spin relaxation times have been measured by the electron-spin resonance technique at microwave frequencies. In a transmission measurement (TESR), a metal foil sample is placed between two microwave cavities, and a large static magnetic field H [3.2 kG for $\omega = 2\pi(9\ \mathrm{GHz})$] is applied. Transverse magnetization is induced (by the microwaves) in the electromagnetic skin on one side of the sample, decays by bulk and surface relaxation processes, and is detected as radiation from within the skin on the opposite side. When $\omega = \gamma H$ (where γ is the gyromagnetic ratio of the electron) the spins precess at the same rate as the rotating, electromagnetic microwave field, and there is resonant transmission. Deviations (of either ω or H) from the resonance condition result in a diminished signal as the spins, which have spent different lengths of time in the interior of the foil, fall out of phase with each other, and the relaxation time T_2 may be deduced from the width of the resonance.[15] The physics is closely related to the Hanle effect and the spin-injection experiment, which are described below. For conduction electron-spin resonance (CESR) one measures the reflected microwave power in a sample cavity. Near resonance, $\omega_L = \gamma H$ (where ω_L is the Larmor frequency and γ is the gyromagnetic ratio), the complex impedance of the sample skin changes rapidly with field or frequency. This is detected as a change in cavity Q and change in reflected power. Again, the relaxation time may be deduced from a width of the resonance.[16]

One disadvantage of ESR is that it must be performed in kilogauss fields. Many metals have g anisotropies which contribute to the relaxation process in appreciable fields, in some instances making the ESR unobservably broad. Many other systems, such as superconductors or spin glasses, have properties of interest that are altered or destroyed in these fields. By utilizing the coupling of charge and spin at a ferromagnetic-paramagnetic interface, one can apply highly sensitive, relatively simple, electronic measurements to probe spin transport at zero or near zero magnetic field.

Briefly the approach is as follows. Spin polarized electrons are injected into a metal bar of thickness d and width a at position $r = 0$. These electrons will diffuse a distance δ_s before losing memory of their initial polarization via a spin relaxation process characterized by the time T_2. The signal at a "spin detector" probe will fall off exponentially with distance from the injector with a characteristic length, essentially δ_s, and the experimental measurement of the signal amplitude versus probe separation will give a direct measure of the spin depth δ_s. However, it is experimentally difficult to prepare a number of nearly identical samples with detectors at increasing distances, just to perform one measurement on each. Alternatively, the Hanle effect,[17] familiar in optical pumping, may be used to measure T_2; the spin magnetization may be destroyed by application of a transverse magnetic field which causes a spin precession. The field effectively randomizes the spins, because spins injected into the metal at different times in the past have accumulated different phases of precession. In the limit of a very small transverse field [$(\gamma B T_2) \ll 1$], each spin precesses only a small angle (much less than 1 rad) before relaxation; all the spins within δ_s at any instant of time will have roughly the same phase (i.e., orientation) as that with which they entered and will contribute coherently to a nonequilibrium magnetization δM. The characteristic field for destruction of the polarization is $(\gamma T_2)^{-1}$. When $\gamma B T_2 > 1$ (a large transverse field), each spin typically precesses more than 1 rad before relaxation. Because spins enter and relax at random times, at any given

instant there will be a broad distribution of spin orientations, and very little net magnetization. There is no longer any phase coherence, and the nonequilibrium magnetization is destroyed. When $\gamma BT_2=1$, the magnetization is diminished by about half its zero field value [for a Lorentzian line, $(\gamma T_2)^{-1}$ is the half width in field at half maximum]. Therefore, a plot of nonequilibrium magnetization as a function of applied transverse field would be a bell-shaped curve, centered at $B=0$.

This is the same physics as TESR, which is a resonant phenomenon performed with frequency and field related by $\omega=\gamma H$. Now, however, the reader must rotate at frequency ω to observe the effect of a deviation of field, ΔH, from the resonant value. All of the electrons acquire an extra phase, with respect to that of the microwave field. The electrons traverse the foil diffusively, and there is a distribution of arrival times at the other surface. When $(\gamma\Delta HT_2)^{-1}=1$, a typical electron has precessed an extra phase of 1 rad before its spin is randomized by a scattering event. There is a distribution of phases of the electrons arriving at the second surface at any given instant. This distribution is shaped, in part, by the scattering frequency $(T_2)^{-1}$. Hence, the signal is diminished for deviations of field (or frequency) from resonance. The TESR line shape relative to the resonant field is essentially the same as the Hanle signal relative to zero field.

Consider the spin-injection approach more carefully. Figure 4 depicts the true geometry of the experiment that we have performed;[1] we have foresaken the pedagogical geometry of Fig. 2 for one which is more readily fabricated, and which has experimental advantages described below. An electric current is driven through a spin polarizing injector at $x=0$ into a thin bar of pure paramagnetic metal. The ferromagnetic film injector and detector previously described serve as spin polarizer and spin analyzer. The moments enter the bar polarized along $\hat{z}$. At $x=L$, a detector measures a voltage V_d proportional to the nonequilibrium magnetization (also along $\hat{z}$, for aligned films) in its vicinity. The electrons diffuse away from the origin in both directions, though eventually all of the electrical current is returned to ground at the left end of the bar. Any drift of the magnetization associated with the electric current is completely negligible compared with the diffusive displacements of the injected spins.

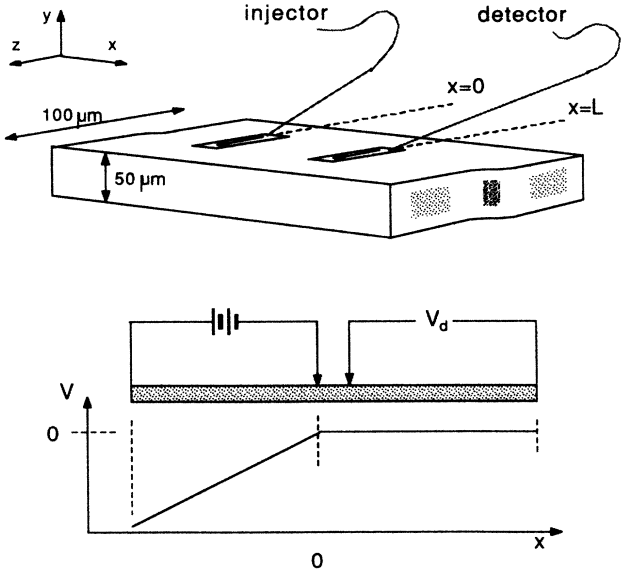

FIG. 4. The true geometry of the spin-injection experiment. There is no classical voltage drop across the detector because there is no net current upstream of the injector.

Notice also that there is no net electrical current for $x>0$. By considering a Fourier expansion solution to Laplace's equations, it can be shown[18] that the right end of the bar and the detector at $x=L$ are very nearly at the same potential. More specifically, for point injector and detector centered on the bar, and for distances long compared to an electronic mean free path (so that ballistic effects are not considered),

$$r_m(L)=\sum_{n=1}\frac{\rho_s}{2\pi n}e^{-n2\pi L/a}\ , \tag{22}$$

where r_m is the classical "mutual" resistance between injector and detector at distance $x=L$, ρ_s is the resistance per square ($\rho_s=4.5\times10^{-7}\ \Omega$ at 4 K for the Al samples), and a is the width of the bar (about 100 μ). For a detector at $L=a$, and for 30 mA drive current, the voltage drop from injector to detector is only a few picovolts. For line injection and detection at $x=0$ and $x=L$, which is more likely the case for our samples, the dimension of the experimental geometry is reduced from three to two, the relevant scale is the thickness of the bar d, and the mutual resistance is given by

$$r_m(L)=\sum_{n=1}\frac{\rho_s}{2\pi n}e^{-n\pi L/d}\ . \tag{23}$$

In our samples $a\approx 2d$, so the leading (and dominant) term is similar in magnitude for each model of the classical voltage distribution.

The spin polarized electrons diffuse away from the origin a characteristic distance δ_s. Within the volume $\Omega\approx ad\delta_s$ the magnetization is given by Eq. (13). A spin analyzing detector at $x=L$ will measure a voltage proportional to this magnetization. In the presence of an externally applied magnetic field (along $\hat{y}$), the response of the magnetization is given formally by the Bloch equations with a diffusion term.[19,20] A quantitative treatment of the problem is given in Appendix B where we solve the Bloch equations with a diffusion term along $\hat{x}$. This one-dimensional model is expected to be valid as long as the spin depth is long compared to the sample thickness, $\delta_s>d$. We will find that the spin depths for all of our data, except those at the highest temperature, obey the condition $\delta_s>a>d$.

The solutions, from Eq. (B21), are found to be

$$V_d=\frac{\eta^2\hbar^2\pi^2(1+b_0)}{e^2m^*k_F}\frac{I_e}{2A}\left[\frac{T_2}{2D}\right]^{1/2}F_i\{\gamma BT_2,L/\delta_s\}\ , \tag{24}$$

where $(1+b_0)^{-1}$ is the Fermi liquid exchange enhancement, m^* is an effective mass, D the electron diffusion constant, k_F the Fermi wave number, A the cross-sectional area of the sample, and the functional form for F_i is given in Appendix B. We will use this expression to fit our experimental results in the following paper.

There is a family of solutions, and a unique solution becomes determined by the relative orientation of the magnetization in the ferromagnetic films. There are two independent solutions of interest, i.e., two functions $F_i\{\gamma BT_2, L/\delta_s\}$. The first, F_1, is plotted in Fig. 5(a) for the parameters of data in Fig. 2 of the following article. Recall from Appendix B that this solution corresponds to the injected magnetization pointing along $\hat{z}$, and the detector measuring magnetization along $\hat{z}$ as well. Thus when the injector and detector are perfectly aligned the signal is "absorptive" in appearance. The second, labeled F_2 in Appendix B, is plotted in Fig. 5(b) for the same parameters. This solution represents injected magnetization along $\hat{z}$, and a detector sensitive to magnetization along $\hat{x}$. In zero field, the detector senses no spin coupled signal because the injector and detector are orthogonal. When a field is applied along $+\hat{y}$, the moments precess in a direction that aligns them with the detector, and a positive signal results. When a field is applied along $-\hat{y}$, the moments precess in a direction that is antiparallel with the detector, and a negative signal is detected. Thus when the injector and detector have their axes of magnetization perpendicular to each other, the injected signal is "dispersive" in appearance. The adjectives absorptive and dispersive are introduced solely because they describe the appearance of the Hanle signal in terms with which the reader may be familiar. They do *not* describe the physics of the signal. For arbitrary alignment, the general solution is a linear combination of F_1 and F_2,

$$V_d \propto F_1 \cos\alpha + F_2 \sin\alpha \ ,$$

where α is the relative angle between injector and detector.

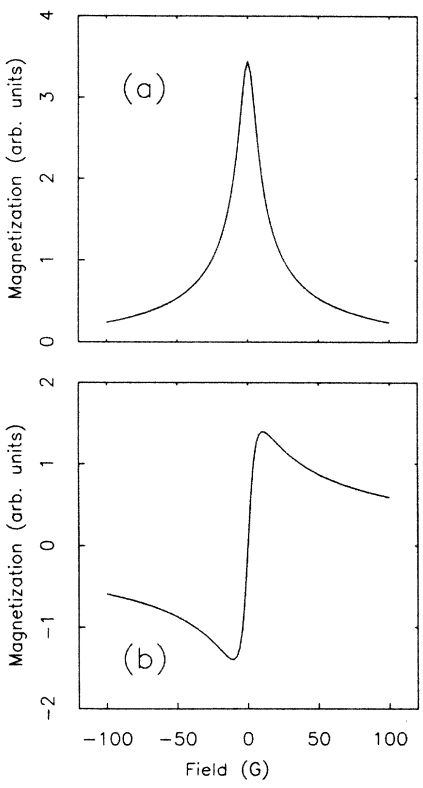

FIG. 5. Magnetization along $\hat{z}$ is injected at $x=0$. (a) The magnetization along $\hat{z}$ at detector $x=L$ as a function of external magnetic field applied along $\hat{y}$, for typical experimental parameters. (b) The magnetization along $\hat{x}$ at detector $x=L$ as a function of external magnetic field applied along $\hat{y}$, for the same parameters as (a).

The parameters appropriate to the curves in Fig. 5 correspond to the limit $L \ll \delta_s$; the probes are closely spaced compared with the spin diffusion length. In this limit the line shape is independent of the electron diffusion constant D, and the width of the line gives the relaxation time T_2. If the inequality is not satisfied, $L \geq \delta_s$, then the line shape is more complicated with sidelobes where the spin coupled signal has reversed sign. The sign reversal occurs at a field such that the spins precess π radians during the mean diffusive transit time between the injector and detector. In this experimental regime, the results can, in principle, be analyzed to give both the conduction electron-spin relaxation time T_2 and the electron diffusion constant D.

Several qualitative features of the predicted Hanle signal can be listed. The amplitude should be directly proportional to the drive current. The signal should be in phase with an audio frequency ac drive current. The signal should appear for applied fields perpendicular to the injected magnetization, i.e., for fields applied along $\hat{x}$ or $\hat{y}$. If the applied field is parallel to the magnetization, along $\hat{z}$, then there will be no torque on the spins and hence no Hanle signal.

The case of a field applied at an angle ϕ from $\hat{z}$ in the $\hat{y}$-$\hat{z}$ plane is analyzed as follows. Recall that the Hanle signal is the result of an applied transverse magnetic field B which causes each moment to precess; when $\gamma BT_2 > 1$ there is no phase correspondence among spins and the net magnetization is destroyed. When an external field, $\mathbf{B}=B\hat{r}$, is applied at angle ϕ, the spins precess about an axis $\hat{r}$ parallel to the field. Let the injected magnetization (in zero field) be $\delta M_0 \hat{z}$. The effect of the field will be to force a precession of δM about the field with a cone of semiangle equal to ϕ. The precession, if $\gamma BT_2 \gg 1$, destroys the component of magnetization perpendicular to B but preserves the component $\delta M \cos\phi$ which is parallel to B. The detector will then sense (when $\gamma BT_2 > 1$) a voltage proportional to the projection of the unaffected magnetization onto the axis of the detector: $(\delta M_0 \cos\phi)(\cos\phi)$. The amplitude of the Hanle signal is proportional to the difference in the magnetization at zero field, which is δM_0, and the magnetization at fields $B > (\gamma T_2)^{-1}$, which is $\delta M_0 \cos^2\phi$. It follows that the Hanle signal amplitude, as a function of field orientation angle ϕ, should vary as

amplitude $(\phi) \propto (\delta M_0 - \delta M_0 \cos^2\phi) = \delta M_0 \sin^2\phi$. (25)

The signal width and shape should be independent of ϕ.

IV. SUMMARY

The concept of electronic spin-charge coupling at a ferromagnetic-paramagnetic interface has been introduced in the contexts of bimetal interfacial transport studies, and of ESR measurements of the conduction electron-spin relaxation time T_2. Microscopic models have been presented to explain how the spin-charge coupling results in spin injection and detection. A framework was developed for analyzing the efficiency of interfacial spin transport in terms of a conductance formula derived in Appendix A. The relaxation time T_2 and diffusion constant D can be measured by application of a small transverse magnetic field which results in a Hanle effect: the diffusing spins are dephased and the magnetization is destroyed. The formal solution to the Bloch equations with a diffusion term is derived in Appendix B. The expected qualitative features of the signal are discussed.

ACKNOWLEDGMENTS

The authors wish to gratefully acknowledge J. Lebens and D. McQueeney for technical assistance, and A. Janossy, H. Hurdequint, P. Monod, and J. Long for useful conversations. This work was principally supported by the National Science Foundation-Materials Research Laboratories program through the Cornell Materials Science Center through Grant No. DMR-8217227; additional help from the Cornell Program on Submicron Structures (PROSUS) and the National Resource and Research Facility for Submicron Structures (NRRFSS) is also acknowledged.

APPENDIX A

We wish to calculate the conductance of an interface between two metals, arriving at a form that we can use in a definition and analysis of the interfacial magnetization transport parameter η. We consider an argument general enough to include both the cases of a tunnel barrier and conduction through small pinholes (hole radius $a \ll$ mean free path l), the Sharvin limit.[21] Some remarks relevant to large pinholes are included at the end of this appendix.

The calculation is done in the context of a single spin subband, the weak transmission limit is assumed so that equilibrium electron distributions may be assumed on either side of the barrier, and the arguments, for the sake of simplicity, are given for the case of no spin orbit mixing of spin and orbital states. The argument does not assume conservation of transverse wave vector as do many of the standard treatments of interface tunneling,[22] in order to allow application to the small pinhole problem (Sharvin limit) as well as to the more general tunneling problem; it is restricted to elastic tunneling. Using a perturbation language and considering the one-electron states to be standing wave states for motion perpendicular to the interface (the $\hat{x}$ direction), we write the current per unit interface area transmitted across the interface from left to right $j_{L\to R}$ as the sum over initial occupied states on the left of transitions to empty states on the right:

$$j_{L\to R} = (-e)\left[\int dE_L \int_{E_L(k_L)=E_L} \frac{L_L}{2\pi\,|\nabla_k E_L(k_L)|}\frac{d^2k_L}{4\pi^2}\frac{2\pi}{\hbar} \times \int dE_R\,\delta(E_L-E_R) \times \int_{E_R(k_R)=E_R} \frac{L_R}{2\pi\,|\nabla_k E_R(k_R)|}\frac{d^2k_R}{4\pi^2}\,|V(k_L,k_R)|^2 f_L(E_L)[1-f_R(E_R)]\right] . \tag{A1}$$

Here L_L is the length of a normalization box for the metal to the left of the interface, $V(k_L,k_R)$ a tunneling (or transmission) matrix element for transfer of an electron from left to right, $E_L(k_L)$ the dispersion relation, and $f_L(E_L)$ the Fermi function for the left metal. Combining this with the corresponding expression for the right to left current, and defining $W(k_L)$, the transition rate through the interface of an electron in state k_L, by

$$W(k_L) = \frac{2\pi}{\hbar}\int dE_R\,\delta(E_L-E_R)\int_{E_R(k_R)=E_R}\frac{L_R}{2\pi\,|\nabla_k E_R(k_R)|}\frac{d^2k_R}{4\pi^2}\,|V(k_L,k_R)|^2 , \tag{A2}$$

the net interfacial current is given by

$$j_{\text{net}} = (-e)\int dE \int_{E_L(k_L)=E}\frac{L_L}{2\pi\,|\nabla_k E_L(k_L)|}\frac{d^2k_L}{4\pi^2}W(k_L)[f_L(E)-f_R(E)] , \tag{A3}$$

where a subscript L has been omitted after performing the integral over the δ function. For the k_L standing wave states we interpret the transition rate $W(k_L)$ as the product of a collision rate (i.e., attempt frequency) with the interface,

$v_x(k_L)/2L$, and a transmission probability $t(k_L)$. Using the assumption of a small applied voltage to replace the difference of the two Fermi functions by a derivative, yields

$$j_{\rm net}=(-e)\int dE \int_{E_L(k_L)=E} \frac{d^2k_L}{8\pi^3 |\nabla_k E_L(k_L)|}\frac{1}{2}|v_x(k_L)|\,t(k_L)(-eV)\left[-\frac{df(E)}{dE}\right]$$
$$=\frac{e^2V}{2}\int_{E_L(k_L)=E_F}\frac{d^2k_L\,|v_x(k_L)|\,t(k_L)}{8\pi^3|\nabla_k E_L(k_L)|}\,. \tag{A4}$$

Noting that the single spin subband density of states may be written as[23]

$$N_L(E)=\int_{E_L(k_L)=E}\frac{d^2k_L}{8\pi^3|\nabla_k E_L(k_L)|}\,, \tag{A5}$$

Equation (A4) may be written in a more intuitively useful form as an interface conductance per unit area,

$$g\equiv\frac{j}{V}=\frac{e^2}{2}N_L(E_F)\langle\,|v_x|\,\rangle_L\langle t\rangle_L\,, \tag{A6}$$

using the definitions

$$\langle v_x\rangle_L\equiv\left[\int_{E_L(k_L)=E_F}\frac{d^2k_L}{8\pi^3}\frac{|v_x(k_L)|}{|\nabla_k E_L(k_L)|}\right]\times[\tfrac{1}{2}N(E_F)]^{-1}\,, \tag{A7}$$

and

$$\langle t\rangle_L\equiv\left[\int_{E_L(k_L)=E_F}\frac{d^2k_L}{8\pi^3}\frac{|v_x(k_L)|\,t(k_L)}{|\nabla_k E_L(k_L)|}\right]\times[\tfrac{1}{2}N(E_F)\langle v_x\rangle_L]^{-1}\,. \tag{A8}$$

Equations (A5)–(A8) give formal meaning to the simple idea that the conductance is proportional to the product of the density of states, an average velocity normal to the interface, and an average transmission probability; and it is an adequate definition for the calculation of interfacial magnetization transport parameter η for a nonideal Stoner ferromagnet, as performed in the text. One could further use this result as a starting point for analyzing and comparing experiments wherein the interfacial transport involves different mechanisms, such as tunneling versus conduction through pinholes, requiring only the assumption of undisturbed Fermi distributions either side of the interface. The principle of detailed balance, which is evident from the symmetry of the expression for the partial current in Eq. (A1), assures that the current could equally well be written in terms of the right-hand metal, i.e.,

$$N_R(E_F)\langle v_x\rangle_R\langle t\rangle_R=N_L(E_F)\langle v_x\rangle_L\langle t\rangle_L\,.$$

For the case of small pinholes ($l<a$) of radius a, with surface density over the interface of N_p, the effective transmission probability is $t'\approx\pi a^2N_p$, or just the fraction of the area covered by pinholes.

Equation (A6) can be further generalized to apply to any band *bs* of the metal, where *b* is the band index (such as 3*d* or 4*s*) and *s* is the spin subband index (up or down):

$$g_{bs}=\frac{e^2}{2}N_{bs}(E_F)\langle v_{x;bs}\rangle\langle t_{bs}\rangle\,, \tag{A9}$$

and this can be used to treat the case of a transition-metal ferromagnet in which more than one band contributes to the conduction.[24] Finally, note that one can make definitions[18] similar to Eq. (A6) that are useful for the analysis of spin transport experiments of entirely different genre, such as spin polarized photoemission spectrometry and inverse photoemission spectrometry.

The preceding calculation is appropriate for the case of small transmission probability, $t\ll1$, such as tunnel junctions or Sharvin pinholes. Another limit of interest is when conductance is restricted by the resistance of the materials; for example, large pinholes (the Maxwell limit, $l>a$). In this case there is an electric field throughout the interfacial region, and one can perform a Boltzmann calculation[25] which is similar to the above derivation. For holes of fractional coverage t' and radius a, the conductance of each hole is approximately the "spreading conductance" σa, and the conductance per unit area is

$$g\approx N_p\sigma a=\sigma a\left[\frac{t'}{\pi a^2}\right]\approx e^2N(E_F)v_Fl\frac{t'}{a}\,. \tag{A10}$$

This is analogous to Eq. (A6) with the interpretation $t\rightarrow t'l/a$.

APPENDIX B

In the experiment depicted in Fig. 4, magnetization is injected with a definite orientation (e.g., along $\hat{z}$) at $x=0$ into a one-dimensional bar (the transverse dimensions are less than a spin depth δ_s). It diffuses away from the origin (along $\pm\hat{x}$) and is eventually relaxed by a T_2 process. In a metal, and in zero field, there is no distinction between a longitudinal relaxation event T_1 and a transverse relaxation process T_2, and we will consider them to be the same. An external field applied along $\hat{y}$ may destroy the magnetization by dephasing the spins. In the limit of a vanishing field, each spin precesses only an infinitesimal amount before relaxation, and all the spins remain at nearly the same phase with which they entered. When $\gamma BT_2>1$, each spin typically precesses more than 1 rad before relaxation. Since spins enter and relax at random times, there is no longer any phase coherence, and the bulk nonequilibrium magnetization is destroyed. This process is closely related to TESR theory,[15] and is described by steady-state solutions to the Bloch equations with a diffusion term along $\hat{x}$, a sink term proportional to $1/T_2$, and a source term (at $x=0$) in the boundary conditions. The Bloch equations,[19] with $\mathbf{B}=B\hat{y}$, are

$$\frac{dM_z}{dt}=-\gamma M_x B-\frac{M_z}{T_2}+D\frac{\partial^2 M_z}{\partial x^2}\ , \tag{B1}$$

$$\frac{dM_x}{dt}=\gamma M_z B-\frac{M_x}{T_2}+D\frac{\partial^2 M_x}{\partial x^2}\ , \tag{B2}$$

$$\frac{dM_y}{dt}=-\frac{M_y}{T_2}+D\frac{\partial^2 M_y}{\partial x^2}\ . \tag{B3}$$

In the spin-injection experiment, magnetization is injected at strictly dc, or at very low audio frequencies (4–20 Hz). However, this need not be the case, and the experiment could be performed at any frequency ω, with the result that the "resonant" field would be shifted up by the usual Larmor relationship $\omega=\gamma H$. We will begin with the most general solution, which is also most closely related to the TESR problem. Thus we anticipate general steady-state solutions that are harmonic in time with frequency ω, take the sum [(B1)+i(B2)], and let $M_+\equiv(M_z+iM_x)=M_{+,0}e^{i\omega t}$ which gives

$$\frac{\partial^2 M_{+,0}}{\partial x^2}=\frac{1}{DT_2}[1+i(\omega-\gamma BT_2)]M_{+,0}\ . \tag{B4}$$

We will seek decaying spatial solutions of the form $e^{\pm\kappa x}$, and define

$$\kappa_+^2\equiv\frac{1}{DT_2}[1+i(\omega-\gamma B)T_2]\ . \tag{B5}$$

Then

$$\kappa_{+\text{real}}=\frac{1}{\sqrt{2DT_2}}\sqrt{1+f(B)}\ ,$$

$$\kappa_{+\text{im}}=\frac{1}{\sqrt{2DT_2}}\frac{(\omega-\gamma B)T_2}{\sqrt{1+f(B)}}\ ,$$

where

$$f(B)=[1+(\omega-\gamma B)^2T_2^2]^{1/2}\ . \tag{B6}$$

There are also solutions to [(B1)−i(B2)]. Letting $M_-\equiv M_z-iM_x$, we have

$$\frac{\partial^2 M_{-,0}}{\partial x^2}=\frac{1}{DT_2}[1+i(\omega+\gamma BT_2)]M_{-,0}\ , \tag{B7}$$

and define

$$\kappa_-^2\equiv\frac{1}{DT_2}[1+i(\omega+\gamma BT_2)]\ , \tag{B8}$$

where

$$\kappa_{-\text{real}}=\frac{\sqrt{1+f(B)}}{\sqrt{2DT_2}}\ ,$$

$$\kappa_{-\text{im}}=\frac{1}{\sqrt{2DT_2}}\frac{(\omega+\gamma B)T_2}{\sqrt{1+f(B)}}\ .$$

The solutions for M_+ and M_- will be given by

$$\begin{aligned}M_+&=A_+e^{\kappa_+x}+C_+e^{-\kappa_+x}\ ,\\ M_-&=A_-e^{\kappa_-x}+C_-e^{-\kappa_-x}\ .\end{aligned} \tag{B9}$$

We now specialize to the case of the dc spin injection experiment, and let $\omega\to 0$. Assume the steady-state boundary condition that at $x=0$ there is a flux of magnetization injected into the region $x>0$ with polarization along $\hat{z}$,

$$\frac{J_{M_z}}{2}=-D\nabla M_z\,|_{x=0}\ , \tag{B10}$$

and there is *no* flux of magnetization with $\hat{x}$ or $\hat{y}$ polarization:

$$J_{M_x}=-D\nabla M_x=0\ \text{ at }\ x=0\ ,$$

$$J_{M_y}=-D\nabla M_y=0\ \text{ at }\ x=0\ .$$

We have used $J_{M_z}/2$ because by symmetry half the injected current diffuses towards $x<0$ and half towards $x>0$. We solve for the half plane $x>0$, and assume that M_i ($i=x,y,z$) vanishes at $x\to\infty$. This implies

$$A_+=A_-=0\ . \tag{B11}$$

It follows that M_z and M_x are given by

$$M_z=\tfrac{1}{2}(M_++M_-)=\tfrac{1}{2}[C_+e^{-\kappa_+x}+C_-e^{-\kappa_-x}]\ ,$$

$$M_x=\frac{1}{2i}(M_+-M_-)=\frac{1}{2i}[C_+e^{-\kappa_+x}-C_-e^{-\kappa_-x}]\ .$$

The above boundary conditions, Eqs. (B10), require

$$\begin{aligned}\kappa_+C_+-\kappa_-C_-&=0\ ,\\ \kappa_+C_++\kappa_-C_-&=\frac{J_{M_z}}{2D}\ .\end{aligned} \tag{B12}$$

Equations (B12) are satisfied by the choice

$$\begin{aligned}C_+&=\left[\frac{\kappa_-}{\kappa_+}\right]^{1/2}C\ ,\\ C_-&=\left[\frac{\kappa_+}{\kappa_-}\right]^{1/2}C\ ,\end{aligned} \tag{B13}$$

and

$$C=\frac{J_{M_z}}{2D\sqrt{\kappa_+\kappa_-}}\ .$$

Substitution of Eqs. (B13) and (B11) into (B9) gives

$$M_+=\frac{J_{M_z}}{2|\kappa_+|^2D}[\kappa_{+\text{real}}-i\kappa_{+\text{im}}]\times e^{-\kappa_{+\text{real}}x}[\cos(\kappa_{+\text{im}}x)-i\sin(\kappa_{+\text{im}}x)]\ , \tag{B14}$$

and

$$M_-=\frac{J_{M_z}}{2|\kappa_-|^2D}[\kappa_{-\text{real}}-i\kappa_{-\text{im}}]\times e^{-\kappa_{-\text{real}}x}[\cos(\kappa_{-\text{im}}x)-i\sin(\kappa_{-\text{im}}x)]\ . \tag{B15}$$

Consider first the case where the spin analyzer is sensitive to magnetization along $\hat{z}$, i.e., along the direction of injection. Then we wish to solve for the z component of magnetization at the position of the detector, M_z $(x=L)$. Note that (for $\omega \to 0$)

$$|\kappa_+|^2=|\kappa_-|^2\equiv|\kappa|^2 ,$$

$$\kappa_{+\text{real}}=\kappa_{-\text{real}},\quad \kappa_{+\text{im}}=-\kappa_{-\text{im}}$$

and (dropping subscript z from J_{M_z} for convenience)

$$M_z=\frac{J_M}{2|\kappa|^2 D}[\kappa_{\text{real}}\cos(\kappa_{\text{im}}L)-\kappa_{\text{im}}\sin(\kappa_{\text{im}}L)]e^{-\kappa_{\text{real}}L} , \tag{B16}$$

where

$$\kappa_{\text{im}}=\frac{1}{\sqrt{2DT_2}}\frac{-\gamma BT_2}{\sqrt{1+f(B)}} ,$$

$$\kappa_{\text{real}}=\frac{\sqrt{1+f(B)}}{\sqrt{2DT_2}} .$$

For the same boundary conditions at $x=0$, one can solve for the x component of magnetization

$$M_x=-\frac{J_M}{2|\kappa|^2 D}[\kappa_{\text{real}}\sin(\kappa_{\text{im}}L)+\kappa_{\text{im}}\cos(\kappa_{\text{im}}L)]e^{-\kappa_{\text{real}}L} . \tag{B17}$$

We can turn these into functions of a reduced field $b\equiv\gamma BT_2$ and a reduced injector-detector separation $l\equiv L/\sqrt{2DT_2}$.

$$M_z=\frac{J_M}{2}\left[\frac{T_2}{2D}\right]^{1/2}\frac{1}{f(b)}\left[\sqrt{1+f(b)}\cos\left[\frac{lb}{\sqrt{1+f(b)}}\right]-\frac{b}{\sqrt{1+f(b)}}\sin\left[\frac{lb}{\sqrt{1+f(b)}}\right]\right]e^{-l\sqrt{1+f(b)}}$$
$$\equiv\frac{J_M}{2}\left[\frac{T_2}{2D}\right]^{1/2}F_1\{b,l\} , \tag{B18}$$

$$M_x=\frac{J_M}{2}\left[\frac{T_2}{2D}\right]^{1/2}\frac{1}{f(b)}\left[\frac{b}{\sqrt{1+f(b)}}\cos\left[\frac{lb}{\sqrt{1+f(b)}}\right]+\sqrt{1+f(b)}\sin\left[\frac{lb}{\sqrt{1+f(b)}}\right]\right]e^{-l\sqrt{1+f(b)}}$$
$$\equiv\frac{J_M}{2}\left[\frac{T_2}{2D}\right]^{1/2}F_2\{b,l\} , \tag{B19}$$

where

$$f(b)=(1+b^2)^{1/2} .$$

Note that $F_1(0,l)=\sqrt{2}e^{-\sqrt{2}l}$, and $F_2(0,l)=0$. Then, inserting (B18) and (B19) into Eq. (21) of the text

$$V_{d;i}=\frac{\eta\beta M}{\chi e}=\frac{\eta^2\beta^2}{\chi e^2}\frac{I_e}{2A}\left[\frac{T_2}{2D}\right]^{1/2}F_i\{b,l\} , \tag{B20}$$

where[20]

$$\chi=\frac{1}{1+b_0}\frac{\beta^2 m^* k_F}{\hbar^2\pi^2} \tag{B21}$$

is the exchange enhanced susceptibility, m^* is an effective mass, and we have used

$$J_M=\frac{\eta\beta}{e}\frac{I_e}{A}$$

with A the cross-sectional area of the sample. Substituting (B21) into (B20) yields

$$V_{d;i}=\frac{\eta^2\hbar^2\pi^2(1+b_0)}{e^2 m^* k_F}\frac{I_e}{2A}\left[\frac{T_2}{2D}\right]^{1/2}F_i\{b,l\} , \tag{B22}$$

which is Eq. (24) in the text. D may be determined from the Einstein relation

$$D=D(T)=\frac{(1+b_0)\sigma_{zz}(T)}{e^2 N^*(E_F)} , \tag{B23}$$

in which $N^*(E_F)$ is the density of states at the Fermi surface, determined by a specific heat measurement, and $\sigma_{zz}(T)$ is the dc conductivity of the sample, which may be measured in a separate experiment on a similarly prepared control sample of comparable dimensions. When one puts in the numbers for the constants, one arrives at

$$V_{d;i}=8.4\times10^{-5}\eta^2\frac{I_e}{A}\sqrt{T_2/D}\,F_i\{b,l\} , \tag{B24}$$

where all units are cgs except V_d and I_e, which are given in volts and amps, respectively. The subscript i in the solution (B24) is to be chosen as 1 (2) when the magnetization of the detector film is chosen to be in the $\hat{z}$ ($\hat{x}$) direction. If the angle between the magnetizations in the two films is α, the function F_i should be replaced by the linear combination $F_1\cos\alpha+F_2\sin\alpha$.

[1]Mark Johnson and R. H. Silsbee, Phys. Rev. Lett. **55**, 1790 (1985).

[2]Mark Johnson and R. H. Silsbee, Phys. Rev. B **35**, 4959 (1987).

[3]A. G. Aronov, Pis'ma Zh. Eksp. Teor. Fiz. **24**, 37 (1976) [Sov. Phys.—JETP Lett. **24**, 32 (1976)].

[4]R. Meservey, D. Paraskevopoulos, and P. M. Tedrow, Phys. Rev. Lett. **37**, 858 (1976).

[5]H. C. Torrey, Phys. Rev. **104**, 563 (1956).

[6]L. D. Flesner, D. R. Fredkin, and S. Schultz, Solid State Commun. **18**, 207 (1976).

[7]Richard Magno and Joe Pifer, Phys. Rev. B **10**, 3727 (1974).

[8]Magno and Pifer (Ref. 7) were the first to perform experiments on the interface in a bimetal sample studying lithium on copper, lithium on manganese, and sodium on aluminum. They analyzed their results using six coefficients in a kinetic model. Their coefficients are directly related to transmission and reflection coefficients. However, there is no experimental configuration that can independently measure any *one* of the coefficients. The results of Fredkin *et al.* may be expressed as linear combinations of Magno and Pifer's coefficients. Magno and Pifer found the probability of electron transmission, with or without spin scattering, to be small, of the order of 10^{-3} or less. They found the probability of spin scattering in a reflection to be temperature dependent; $\varepsilon=\varepsilon(T)$ which is of the order of $(1-20)\times10^{-3}$. Flesner *et al.* used reflection and transmission ESR on lithium on copper samples to probe the interface. When they interpret their results in terms of a kinetic model, they find a single probability, $\varepsilon=2.5\times10^{-3}$, for a spin relaxation for any interaction with the surface, and a probability of $t=0.02$ for an electron to cross the interface with or without spin scattering. We will neglect interfacial spin relaxation as a negligible effect.

[9]P. M. Tedrow and R. Meservey, Phys. Rev. Lett. **26**, 192 (1971).

[10]P. M. Tedrow and R. Meservey, Phys. Rev. B **7**, 318 (1973).

[11]R. H. Silsbee, Bull. Magn. Res. **2**, 284 (1980).

[12]Most generally, $\mathbf{J}_e$ is a vector and $\overleftrightarrow{\mathbf{J}}_M$ is a second-rank tensor; the component $(J_M)_{ij}$ describes the transport along the jth axis of the projection of the magnetization on the ith axis. Under the simplifying assumptions that J_e is normal to the interface, that the magnetization of the film is in the plane of the film along a direction $\hat{m}$, and that J_M is oriented along $\hat{m}$, both J_e and J_M may be treated as scalars.

[13]Note that η can have either sign; in the simplest picture of Fig. 2(b) we see that it is positive (negative) if the minority (majority) spin subband has a larger density of states at the Fermi surface. Thus, one could use subscripts $^{\text{maj}}_{\text{min}}$ interchangeably with $^{\text{down}}_{\text{up}}$ in the ferromagnet. The former are more informative than the latter, because the majority subband is well defined by the direction of equilibrium magnetization, and then the sign of η would identify which subband is dominating the transport. However, $^{\text{maj}}_{\text{min}}$ are inappropriate in the paramagnet. In order to avoid confusion, we will use the arbitrary choice $^{\text{down}}_{\text{up}}$ throughout.

[14]In the following, we will use the free electron value $g=2$.

[15]Richard B. Lewis and Thomas R. Carver, Phys. Rev. **155**, 309 (1967).

[16]Freeman J. Dyson, Phys. Rev. **98**, 349 (1955).

[17]W. Hanle, Z. Phys. **30**, 93 (1925).

[18]Mark Johnson, Ph.D. dissertation, Cornell University, 1986.

[19]N. S. VanderVen and R. T. Schumacher, Phys. Rev. Lett. **12**, 695 (1964).

[20]P. M. Platzman and P. A. Wolff, *Waves and Interactions in Solid State Plasmas* (Academic, New York, 1973), Eq. (53.25).

[21]A. G. M. Jansen *et al.*, J. Phys. C **13**, 6073.

[22]C. B. Duke, *Tunneling in Solids* (Academic, New York, 1969), Suppl. 10.

[23]Neil W. Ashcroft and N. David Mermin, *Solid State Physics* (Holt, Rinehart and Winston, New York, 1976), Eqs. (2.21), (2.86), and (8.63).

[24]We have been neglecting interfacial spin relaxation. However, we could include this effect by defining a conditional probability that a spin which is transmitted has not undergone a spin flip interaction in the process; this probability would most generally be different for each subband *bs*.

[25]J. M. Ziman, *Principles of the Theory of Solids*, 2nd ed. (Cambridge University Press, Cambridge, 1972), p. 215.

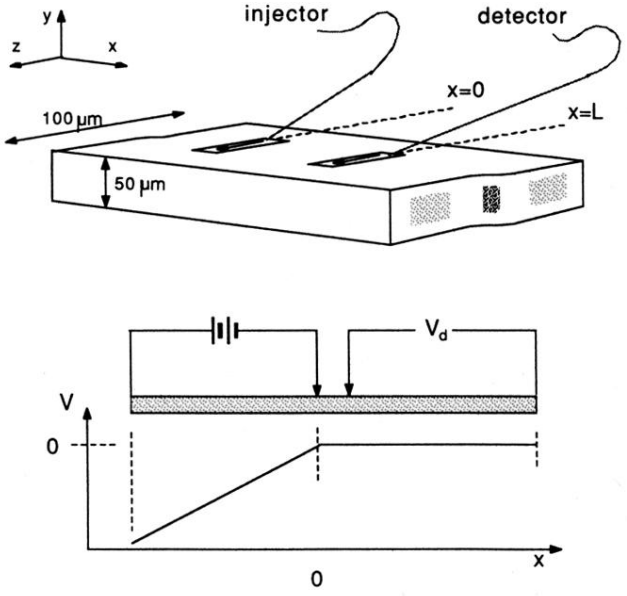

FIG. 4. The true geometry of the spin-injection experiment. There is no classical voltage drop across the detector because there is no net current upstream of the injector.